Seasonal plasticity in the adult somatosensory cortex

Saikat Ray[a,b,1], Miao Li[c,d], Stefan Paul Koch[e,f], Susanne Mueller[e,f], Philipp Boehm-Sturm[e,f], Hong Wang[c,d], Michael Brecht[a], and Robert Konrad Naumann[c,d,1]

[a]Bernstein Center for Computational Neuroscience, Humboldt University of Berlin, 10115 Berlin, Germany; [b]Department of Neurobiology, Weizmann Institute of Science, 7610001 Rehovot, Israel; [c]Chinese Academy of Sciences Key Laboratory of Brain Connectome and Manipulation, The Brain Cognition and Brain Disease Institute, Shenzhen Institutes of Advanced Technology, Chinese Academy of Sciences, 518055 Shenzhen, People's Republic of China; [d]Shenzhen-Hong Kong Institute of Brain Science-Shenzhen Fundamental Research Institutions, 518055 Shenzhen, People's Republic of China; [e]Department of Experimental Neurology and Center for Stroke Research, Charité – Universitätsmedizin Berlin, 10117 Berlin, Germany; and [f]NeuroCure Cluster of Excellence and Charité Core Facility 7T Experimental MRIs, Charité – Universitätsmedizin Berlin, 10117 Berlin, Germany

Seasonal cycles govern life on earth, from setting the time for the mating season to influencing migrations and governing physiological conditions like hibernation. The effect of such changing conditions on behavior is well-appreciated, but their impact on the brain remains virtually unknown. We investigate long-term seasonal changes in the mammalian brain, known as Dehnel's effect, where animals exhibit plasticity in body and brain sizes to counter metabolic demands in winter. We find large seasonal variation in cellular architecture and neuronal activity in the smallest terrestrial mammal, the Etruscan shrew, *Suncus etruscus*. Their brain, and specifically their neocortex, shrinks in winter. Shrews are tactile hunters, and information from whiskers first reaches the somatosensory cortex layer 4, which exhibits a reduced width (−28%) in winter. Layer 4 width (+29%) and neuron number (+42%) increase the following summer. Activity patterns in the somatosensory cortex show a prominent reduction of touch-suppressed neurons in layer 4 (−55%), the most metabolically active layer. Loss of inhibitory gating occurs with a reduction in parvalbumin-positive interneurons, one of the most active neuronal subtypes and the main regulators of inhibition in layer 4. Thus, a reduction in neurons in layer 4 and particularly parvalbumin-positive interneurons may incur direct metabolic benefits. However, changes in cortical balance can also affect the threshold for detecting sensory stimuli and impact prey choice, as observed in wild shrews. Thus, seasonal neural adaptation can offer synergistic metabolic and behavioral benefits to the organism and offer insights on how neural systems show adaptive plasticity in response to ecological demands.

seasonal adaptation | adult cortical plasticity | somatosensory cortex | shrews | Dehnel's effect

Animals have evolved to display extraordinary ethological adaptations in response to the ecological variations they face. Monarch butterflies perform annual migration cycles, each of which is completed over several generations (1), while squirrels can hibernate for several months (2). The primary organ responsible for regulating behaviors, the brain, also exhibits the ability to change: In response to environmental changes, behavioral needs, injury, or to form new memories (3–6). While the consequences of such neural plasticity have been studied at the synaptic level, minute changes in neuronal and synaptic activity over short time-scales, the impact of longer-term behavioral variations on neural structure and activity is largely unknown. Notable exceptions are songbirds that display seasonal variation in song repertoire and correlated anatomical changes in song nuclei (7). Although seasonal brain plasticity has mostly been studied in birds, mammalian brains, including humans (8), also display such effects. However, the evolutionary relations between key bird and mammalian brain regions are disputed (9, 10). Some of the most drastic yet largely unexplored seasonal changes in brain structure have been observed in small mammals, like shrews and weasels (11, 12). This phenomenon is known as Dehnel's

effect and entails a reduction in body weight, skull, and brain size during autumn and winter (11–15). We explore this effect in Etruscan shrews and find that individual shrews exhibit seasonal changes in brain size, with the cerebral cortex shrinking in winter. We then determine the microanatomical substrate of such cortical volume changes and report evidence of seasonal changes in neural activity in the cerebral cortex.

Results

To determine whether individual animals exhibited seasonal changes in brain volume, we performed repeated in vivo magnetic resonance imaging (MRI) scans of the same shrews (Fig. 1A and *SI Appendix*, Fig. S1 A and B) over the period of a year. The scans were performed starting from summer across different seasons (Fig. 1A) and indicated that the brain volume of shrews decreased in autumn and winter (Fig. 1C and *SI Appendix*, Fig. S1C and Table S1), despite the shrews being housed in constant temperature, photoperiod, and ad libitum food conditions throughout the year. We also performed in situ MRI scans of shrews at different ages and weights (*SI Appendix*, Fig. S2 A and B) and determined that brain volume was correlated with both age and weight (*SI Appendix*, Fig. S2C). On normalizing the brain

Significance

To survive, animals need to adapt to changes of their ecosystem by changing their behaviors or even morphing the organs responsible for generating these behaviors. Small mammals have a high metabolic rate, and to balance energy deficits during winter they can decrease their brain and body size, a phenomenon termed Dehnel's effect. We find specific seasonal changes in the brain of the smallest terrestrial mammal, the Etruscan shrew. Their cortex shrinks in the winter, with layer-width and neuron number reduction in the energetically expensive somatosensory cortical layer 4. Imaging of neural activity revealed reduced suppressive responses to whisker touch during winter, indicating that such cortical adaptation may have synergistic functional and behavioral effects in addition to direct metabolic benefits.

Fig. 1. Seasonal shrinkage of the brain and cortex. (*A*) Noninvasive brain imaging of Etruscan shrews was performed over different seasons using 7-Tesla MRI with cryoprobe. The brain (gray) of the same Etruscan shrew imaged over different seasons with the cortex highlighted: Summer (orange), autumn (magenta), winter (blue), and spring (green). Shrew illustration adapted from ref. 18, which is licensed under CC BY 4.0. (*B*) Superimposition of the cortex of the same shrew imaged in winter (blue) onto the summer (orange) image shows that the cortex volume decreases in winter (mostly orange is visible, indicating a larger summer cortex). (*C*) The brain of shrews (*n* = 10 shrews) shrinks during autumn and winter and recovers the following spring (black dots indicate means). (*D*, *Upper*) The cortex of shrews (*n* = 10 shrews) becomes smaller in the autumn and winter seasons and recovers slightly the following spring. (*Lower*) The average weight of the shrews increases, despite a reduction of the cortex during autumn and winter (black dots indicate means and gray shaded area indicates SEM). (*E*) Schematic indicating the radial and cortical surface axis of the cortex, the longitudinal axis is indicated in *B*. (*F*) Changes in cortical volume are not isotropic, with a reduction of the cortex along the radial and longitudinal directions, but not the cortical surface axes (*n* = 9 shrews). The lengths of the boxes indicate the percentages of increases or decrease along the radial and longitudinal directions, and cortical surface. For statistical information, see *SI Appendix*, Table S1.

volumes by age and weight based on a generalized linear model (*SI Appendix*, Fig. S2D), we determined that the reduction in brain volume during autumn and winter was even more pronounced (*SI Appendix*, Fig. S2E and Table S1). We then delineated brain structures from the T2-weighted MRI images (*SI Appendix*, Fig. S1 *A* and *B*) using expert-user and automated segmentation to determine which regions of the brain showed a reduction in volume during the winter period (*SI Appendix*, Fig. S1 *C–H*). We found that only the cerebral cortex consistently shrank during the winter period (Fig. 1 *B* and *D* and *SI Appendix*, Fig. S1D and Table S1), despite an overall growth of the shrew (Fig. 1D). We did not find evidence of this seasonal plasticity in the remaining brain regions: Olfactory bulb, hippocampus, cerebellum, and other subcortical areas (*SI Appendix*, Fig. S1 *E–H* and Table S1). To determine if the reduction in cortex volume was isotropic, we measured changes at specific locations at the cortex (*SI Appendix*, Table S2) from summer to winter in the same animals along the different axes of the cortex (Fig. 1 *B* and *E* and *SI Appendix*, Fig. S3). We found that the changes were not isotropic, with the cortex shrinking in the radial and longitudinal axes but increasing along the cortical surface axis (Fig. 1F).

To understand the neural underpinnings of these cortical volume changes, we performed a microstructural analysis of the shrew neocortex. The Etruscan shrew has the smallest mammalian cortex, with an average thickness of ~500 μm (Fig. 2A) (16). We found that the cortex of the shrews was 9.9 ± 1.7% thinner during winter than summer (Fig. 2A) (mean ± SEM) by investigating the motor cortex, visual cortex, and somatosensory cortex (Fig. 2B and *SI Appendix*, Fig. S4 *C* and *D*). As the somatosensory cortex is one of the largest parts of the shrew cortex (16) and the sense of touch is crucial to the shrew for prey capture, and thus survival (17, 18), we investigated further changes in this cortical region. Despite the diminutive size of the Etruscan shrew cortex, six layers are readily identifiable in Nissl stains (Fig. 2A). Layer-specific histochemical, immunohistochemical, and gene-expression markers (Fig. 2C and *SI Appendix*, Fig. S4 *A* and *B*) reveal a laminar layout similar to other mammals. In addition, similar to other mammals (19–22) but unlike some rodents (*SI Appendix*, Fig. S5A), the shrews lacked anatomically defined whisker-barrels in layer 4 (*SI Appendix*, Fig. S5 *B–E*). However, changes in somatosensory cortical thickness were layer-specific, and layer 4 showed a significant change in size from summer to winter, decreasing in thickness by 27.9% during winter (Fig. 2D and *SI Appendix*, Table S1) in shrews <1 y old, and increasing again in older shrews by 28.6% (Fig. 2D and *SI Appendix*, Table S1) in their second summer. Changes in neuron numbers contributed to this increasing thickness in the second summer, with columnar neuronal density in layer 4 being 42.38% higher in the second summer than in winter (age of summer shrews = 18.6 ± 2.4 mo, winter shrews = 6.6 ± 1.1 mo; $n = 10$ shrews, $P = 0.012$, two-tailed Mann–Whitney U test; mean ± SEM), despite no significant change in overall volumetric neuronal density. (Fig. 2 *E* and *F* and *SI Appendix*, Table S1).

We then investigated if the structural changes in the somatosensory cortex between autumn–winter and spring–summer are also accompanied by changes in neuronal responses. To determine this, we performed in vivo two-photon imaging in the somatosensory cortex while stimulating individual contralateral whiskers with a piezoelectric actuator (Fig. 3A). Calcium signals from neurons across layers 2 to 5 (*SI Appendix*, Figs. S6 and S7) were recorded using Oregon Green BAPTA (OGB) (Fig. 3B). The calcium signal was de-noised and responses of each neuron to whisker stimulation were determined both directly from the de-noised signal (*SI Appendix*, Fig. S8) and inferred calcium events (Fig. 3C). Cells that responded reliably to whisker stimulation and showed a higher or lower firing rate at the 95th-percentile level in response to stimulation were classified as being activated or suppressed upon touch, respectively (Fig. 3 C

and *D* and *SI Appendix*, Figs. S7C and S8). We imaged the activity of 1,248 neurons (Fig. 3D), and found neurons that were significantly activated, suppressed, or unmodulated (Fig. 3 *D* and *E*) upon whisker stimulation in all layers (*SI Appendix*, Figs. S7 and S8). On exploring the differences between touch responses during summer and winter, we found a consistently lower fraction of neurons were suppressed during winter, with the proportion of touch-suppressed neurons increasing 54% during the spring–summer period (Fig. 3F and *SI Appendix*, Fig. S8 and Table S1). Furthermore, concomitant with the structural changes, layer 4 had the most pronounced effect, where the fraction of neurons suppressed during spring-summer was 2.3-fold higher than that in autumn–winter (Fig. 3G and *SI Appendix*, Fig. S8).

What factors could underlie the structural and functional effects observed in layer 4 somatosensory microcircuits? Layer 4 shows the highest cytochrome oxidase activity in the somatosensory cortex (Fig. 4A), an indicator of metabolic activity (23), and a reduction in number of neurons in layer 4 can most efficiently offer direct metabolic benefits. One of the most active (24), and thus energetically expensive neuronal subtypes (25) in this layer are parvalbumin-positive (PV^+) interneurons (Fig. 4B), and we found that there were fewer PV^+ interneurons in winter (Fig. 4 *B* and *C* and *SI Appendix*, Table S1). As PV^+ interneurons are also the key mediators of layer 4 cortical inhibition (26), the lower number of PV^+ interneurons during winter could contribute to the drastic decrease in suppressive neuronal responses to touch during winter. However, since PV expression in neurons can itself be modulated by the activity level of neurons (27), the causality between fewer detected PV^+ interneurons and cortical activity level needs to be directly determined. The impact of a compromised inhibitory structure on neuronal responses is also consistent with the slower decline in poststimulation attenuation in neuronal activity during the autumn–winter months (*SI Appendix*, Fig. S9).

We then examined if changing an external signal related to metabolism, like food availability, can induce a similar effect. We varied the food available to the shrews during the same season (summer) and found that the shrews had a decline in brain and cortex volume (Fig. 4 *D* and *E*), but not in other brain areas during periods of restricted food availability. This was despite a general growth of the shrew (weight of shrew with abundant food 2.27 ± 0.08 g, limited food 2.80 ± 0.16 g, $n = 7$ shrews, $P = 0.007$, two tailed paired t test, mean ± SEM), similar to the seasonal plasticity they display in winter (Fig. 1 *C* and *D*).

Discussion

Animals can show remarkable adaptations to combat adverse conditions (28, 29), despite the absence of explicit external cues (2). In nature, when such adaptations occur together with other triggers like food, photoperiod, and temperature variations, which can induce further acclimatization (15), the overall effect could be even larger (11). In the laboratory, even in the absence of direct seasonal cues, the shrews might inherit temporal cues through changes in odors of their prey, as has been observed in other species (30) or evolved endogenous annual timekeeping mechanisms (2, 31). Shrews have a thinner cortex in the winter than summer, and the increase during the following spring also happens along the radial axis of the cortex, with an increase of laminar thickness and columnar neuronal density. These changes may involve neurogenesis, as observed in songbirds (7), or a type conversion from astrocytes to neurons by up-regulation of selected genes, as demonstrated in the adult rodent cortex (32). Small mammals like the Etruscan shrew have exceptionally high metabolic rates but low energy reserves (33), and a reduction in brain size aids survival during periods of low food availability, like winters in the wild. A lower number of neurons in the energetically expensive layer 4 (34) can offer direct metabolic benefits; however, the neurobiological effect of such an adaptation on
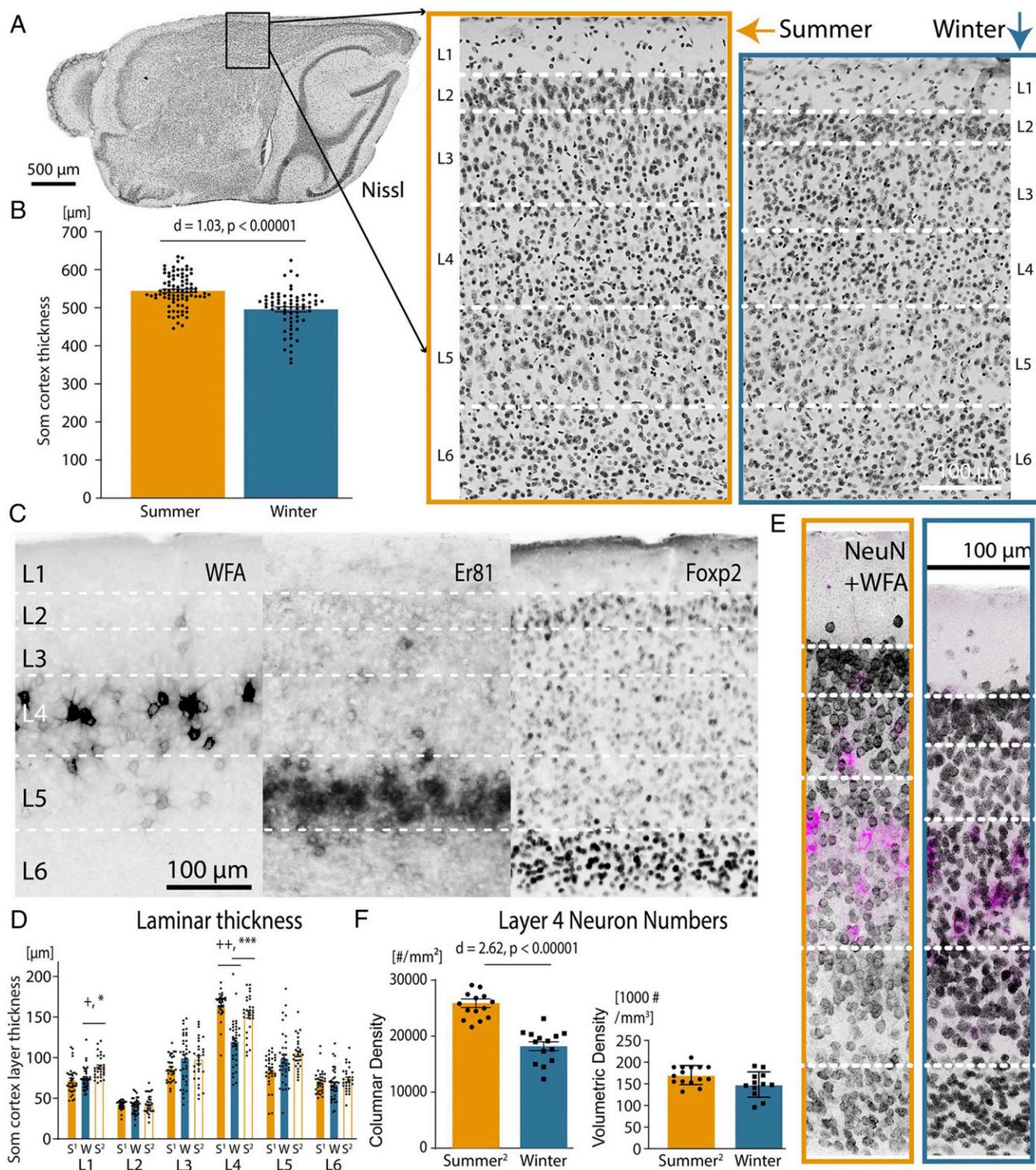
Fig. 2. Cortical and laminar seasonal changes in somatosensory cortex. (*A*) Parasaggital section showing the somatosensory cortex (Som) in Nissl-stained sections in summer (orange box) and winter brains (blue box), showing a thinning in layer 4 in the winter. (*B*) The somatosensory cortex is thicker in summer than in winter (*n* = 10 shrews). Error bars are mean ± SEM. (*C*) Histochemistry (WFA), immunohistochemistry (Foxp2), and gene expression (Er81) aid to distinguish cortical layers and generally show the same laminar distribution as in other mammals, despite much lower cortical thickness. (*D*) Layer 4 of the somatosensory cortex shrinks from summer (S[1], age Summer[1] shrews = 7 ± 2 mo) to winter (W, age Winter shrews = 10.7 ± 2.8 mo) in the first year of the shrew, and grows in the second summer (S[2], age Summer[2] shrews = 18.6 ± 2.4 mo) (*n* = 15 shrews). [+]*d* > 0.8, [++]*d* > 1.2, *P < 0.001, ***P < 0.00001, Bonferroni-corrected α = 0.004. Error bars and ages are mean ± SEM. (*E*) NeuN immunohistochemistry on shrew brains from summer (orange box), and winter (blue box) demonstrates shrinkage in layer 4 in the winter. Layer 4 can be easily discriminated by costaining with layer 4-specific marker WFA (magenta). (*F*) Layer 4 of the somatosensory cortex has lower columnar neuron density (*Left*) but not volumetric density (*Right*) in the winter (*n* = 10 shrews). Error bars are mean ± SEM. For statistical information, see *SI Appendix*, Table S1.
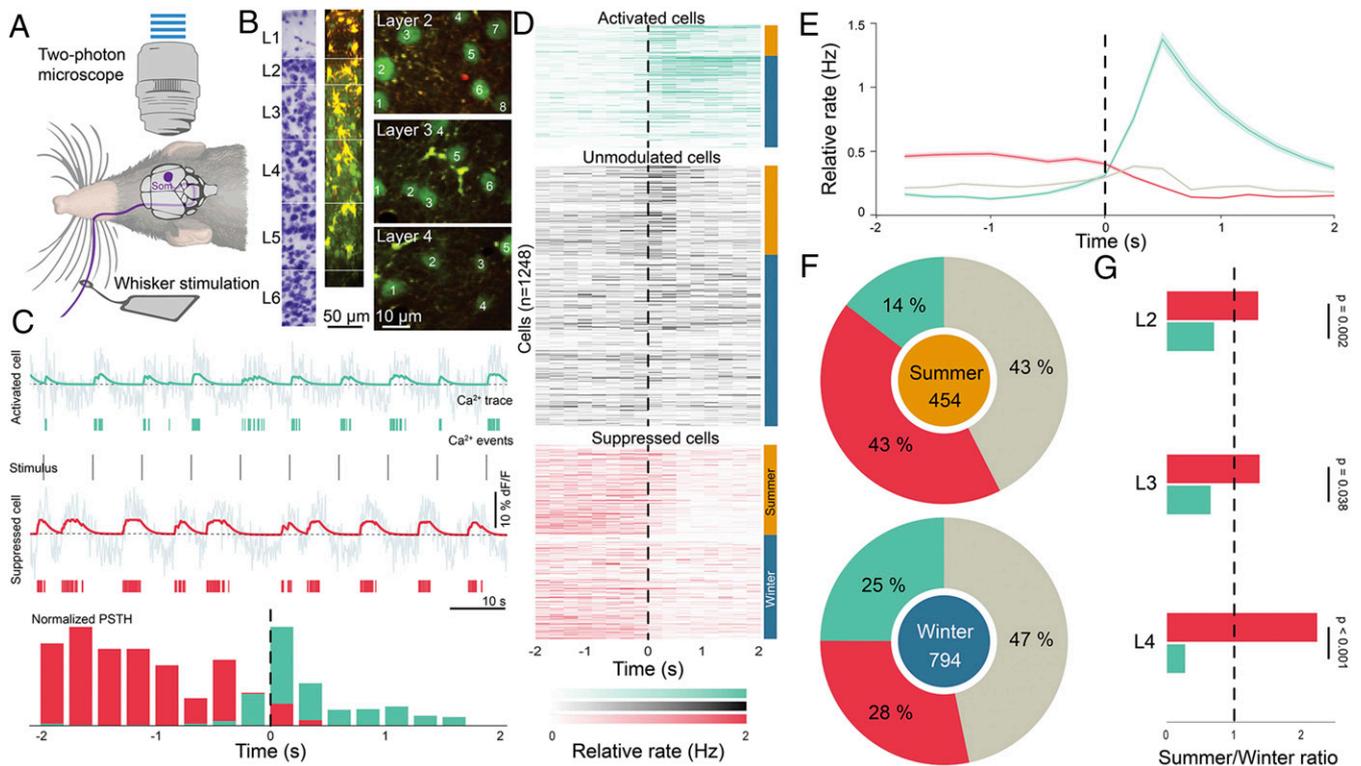
Fig. 3. Reduced suppression of neurons in the somatosensory cortex during the autumn–winter period. (*A*) Schematic illustrating two-photon imaging of Etruscan shrews during whisker stimulation. (*B*) Two-photon imaging was performed using OGB in layers 2 to 5 of the shrew primary somatosensory cortex. (*C*) Examples of simultaneously recorded cells that are either activated (green) or suppressed (red) on whisker stimulation. (*Top*) Raw calcium signal in gray with smoothed signal (green) superimposed on it of a cell activated on whisker stimulation. (*Middle*) Calcium events inferred from the calcium trace (green lines) and whisker stimulus (gray). Similarly, calcium trace and inferred calcium events (red) of a cell suppressed on whisker stimulation. (*Bottom*) Normalized PSTH of the two cells locked to whisker stimulation over the whole experiment. Vertical scale bars correspond to 10% dF/F and horizontal scale bars to 10 s. (*D*) Responses of all neurons recorded in the somatosensory cortex ($n = 1,248$ cells, 12 shrews) aligned to whisker stimulation (black line) and classified as activated (green), unmodulated (gray), or suppressed (red) on whisker stimulation based on their z-scores. The cells recorded during summer are indicated with an orange bar at the side, and the ones in winter with a blue bar. (*E*) Mean (line) ± SEM (shaded area) of responses of all activated (green), suppressed (red), and unmodulated cells (gray) in the somatosensory cortex aligned to stimulus onset. (*F*) Summary of responses during spring-summer (*Upper*; orange, $n = 454$ cells, 5 shrews) or autumn–winter (*Lower*; blue, $n = 794$ cells, 7 shrews) periods indicate that a larger fraction of cells in S1 are suppressed (red) on whisker stimulation during summer ($P < 0.001$, z-test) compared to winter. (*G*) Summer-to-winter ratios of suppressed and activated cells across layers 2 to 4 indicate that layer 4 shows the most pronounced differential effects between the two seasonal periods, with a larger fraction of suppressed neurons during summer than in winter. For statistical information, see *SI Appendix*, Table S1.

the organism could be multifaceted. We find that the thinner winter cortex also displays radically different neuronal responses to touch, indicating an extreme seasonal change in the cortical coding scheme. A decrease in touch-suppressed neuronal responses could indicate a compromised center-surround balance of whisker responses (35), influencing the threshold for detecting sensory stimuli and consequently, prey choice, a behavior that has been observed in shrews in the wild. In summer, shrews mostly prefer to eat earthworms but completely avoid similarly shaped millipedes; however, in winter they lose this specificity and eat comparable amounts of both (36). Thus, reducing cortical size during food shortage could be beneficial, not only for balancing metabolic energy deficits but also by providing a neurobiological adaptive benefit for foraging under adverse conditions (37). Taken together, our findings suggest that Etruscan shrews sacrifice early sensory cortical processing and inhibitory sensory gating in order to survive winter.

Materials and Methods

All experiments were performed according to German guidelines on animal welfare under the supervision of the local ethics committees (Landesamt für Gesundheit und Soziales, Berlin; Permit numbers: G0170/15, T0160/14 and T0078/16).

Experimental Animals. In this study we included 100 adult Etruscan shrews (*Suncus etruscus*) of both sexes. All shrews were born in an in-house colony, with breeding terraria containing a large block of plaster containing a system of tunnels functioning as potential breeding chambers (17). Shrews were subsequently housed in terraria containing a layer of dry soil, moss, stones, and pieces of wood and broken flowerpots. Their diet consisted of live food of crickets, mealworms, and water ad libitum. For experiments related to limited food conditions, shrews received six to eight crickets per day. Light cycle was constant throughout the year with 12 h of light and dark phase each, and ambient temperature was maintained at 20.83 ± 0.07 °C and relative humidity at 48.17 ± 0.56% (mean ± SEM). The year was demarcated into four seasons based on the calendar date of the year: Spring (21 March to 20 June), summer (21 June to 22 September), autumn (23 September to 20 December), or winter (21 December to 20 March).

Magnetic Resonance Imaging. MRI was performed in situ and in vivo at a 7 Tesla rodent scanner (BioSpec 70/20 USR; Bruker) running Paravision 6.0.1 software with a 20-cm horizontal bore magnet and a shielded gradient system (11.4-cm inner diameter, maximum gradient strength 440 mT/m). A mouse head transmit/receive 1H-CryoprobeTM (Bruker) allowed data acquisition with two to three times higher signal-to-noise ratio compared to conventional room-temperature coils. For whole-brain high-resolution morphological imaging, a T2 weighted turbo spin echo sequence was used with a volumetric resolution of 0.00145 mm³ (2D RARE, 36 contiguous slices, 0.25 mm slice thickness, field of view 12.8 × 12.8 mm², in plane resolution 75 × 75 µm², repetition time 4,000 ms, echo time spacing 11.5
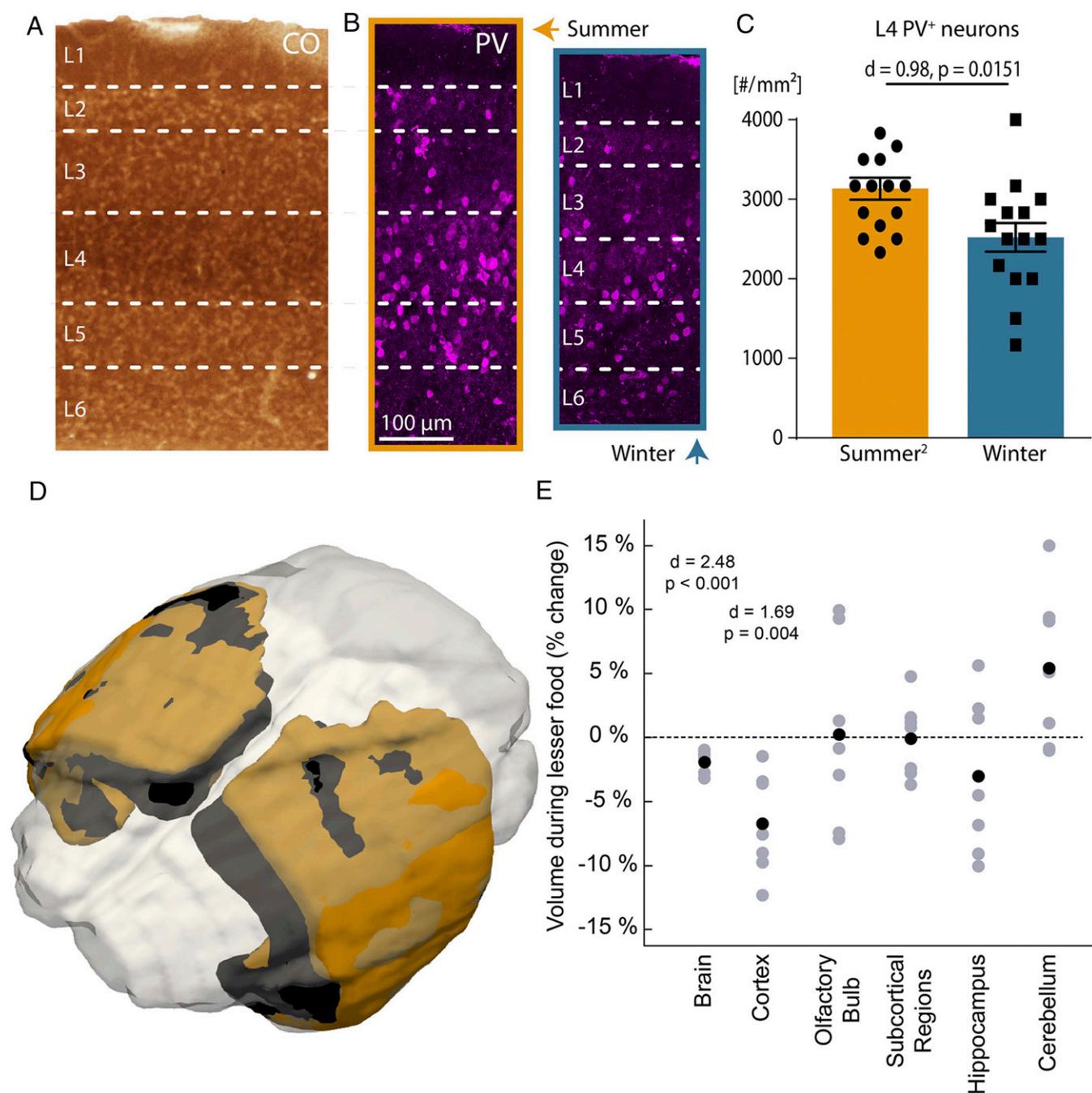
Fig. 4. Energetically expensive layers of the somatosensory cortex, and cortex-specific reduction of brain volume induced by less food independent of season. (*A*) Cytochrome oxidase histochemistry indicates that layer 4 of the somatosensory cortex is the most metabolically active layer. (*B*) Immunohistochemical processing for PV$^+$ neurons in summer (orange box) and winter (blue box) shows lower PV$^+$ neurons in winter. (*C*) Columnar density of layer 4 PV$^+$ neurons in winter compared to summer ($n = 10$ shrews). Error bars are mean $\pm$ SEM. (*D*) Superimposing the cortex of the same shrew imaged from a summer when it had abundant food (orange) to one with limited food (black) shows a decline in brain volume when having limited food (mostly orange is visible). (*E*) The brain and cortex of the same shrews ($n = 7$ shrews), but not other brain areas, reduce in volume when they have lesser food during the same seasonal period (summer). Black dots indicate means. For statistical information, see *SI Appendix*, Table S1.

ms, effective echo time 34.5 ms, RARE factor 8, 10 averages, total acquisition time 14:00 min). For in vivo imaging, shrews were anesthetized with 1 to 2% isoflurane under constant ventilation monitoring. In situ imaging was performed directly after sacrificing shrews with a high dose of isoflurane.

MRI Segmentation, Visualization, Volume, and Distance Measurements. Manual segmentation and volumetry of brain structures was done in a blind design with Analyze 10.0 software (AnalyzeDirect). Expert-user segmentations were made on the raw T2-weighted images, based on clearly defined borders determined by white matter or ventricles.

For automatic segmentation, all MR images were processed in MATLAB (Mathworks) toolbox ANTX2 based on SPM functions and elastix (38, 39). An average shrew brain template was generated including tissue probability maps of gray matter, white matter, and cerebrospinal fluid in a four-step iterative method starting from C57/Bl6 mouse tissue probability maps using a unified segmentation approach (38–41). The resulting average shrew brain template, based on 48 shrew brain scans, was processed with ANTX2 and is

publicly available (https://github.com/ChariteExpMri/antx2). Individual T2-weighted images of shrew brains were registered with ANTX2 to this template using a nonlinear transformation. Brain structures for each shrew brain were automatically segmented based on the transformation of manually segmented regions of a reference animal to the template and the respective inverse transformation to each shrew brain scan from the average template.

Multiple individual experimenters and automated segmentation had a high degree of correspondence in delineating the segmented regions with 87.71 ± 2.30% similarity (dice coefficient) between experimenters and 85.63 ± 1.22% similarity (mean ± SEM) between experimenter and automated segmentation (42, 43). The average changes determined from the manual and automated measures are used with the individual values derived from each measure presented for comparison in SI Appendix, Fig. S1.

For visualization only, individual images were coregistered and resliced with trilinear interpolation to a reference scan that was chosen due to very symmetric alignment inside the scanner with normalized mutual information as a cost function. To ensure that the coregistration conserved potential volume differences, a rigid body transformation (six degrees of freedom: three translational and three rotational) was applied. The coregistration function found for the T2-weighted image was then applied to the corresponding masks of delineated brain structures using nearest neighbor interpolation. The differences in volumes of the coregistered masks were visualized as three-dimensional (3D) renderings using ITK-SNAP and Paraview (NTESS).

To determine changes along different cortical axes, nodes were marked in standard shrew space coordinates on the shrew brain template (SI Appendix, Table S2). Images were upsampled to $20 \times 20 \times 20$ μm^3 isometric resolution to determine the changes in the same shrews between pairs of these nodes imaged in summer and winter. The brains were aligned with the registration method described above to determine the changes between these specific nodes in the radial and longitudinal directions (SI Appendix, Fig. S3 A and C). Along the cortical surface axes, the changes were determined for the piecewise sum of the distances between consecutive nodes (SI Appendix, Fig. S3B). The median changes across animals at each of these 24 locations per axes was used to determine the change in cortex from summer to winter.

Brain Tissue Preparation. Brain tissue was prepared as described previously (16, 44). Using isoflurane, Etruscan shrews were briefly anesthetized and subsequently given an intraperitoneal injection of 20% urethane. We perfused animals with 0.9% PBS solution and 4% paraformaldehyde (PFA) in 0.1 M phosphate buffer (PB). Subsequently, brains were dissected out and fixed again in PFA overnight. For long-term storage, brains were transferred to a solution of 0.1% sodium azide in 0.1 M PB. Before sectioning, shrew brains were cryoprotected using an ascending series of 10% and 30% sucrose solution in PB, each step lasting at least 24 h. We used Jung Tissue Freezing Medium for embedding brains and prepared 60-µm-thick sagittal sections.

Histochemistry and Immunohistochemistry. Sections were processed for histochemistry, including Nissl staining and cytochrome oxidase staining (23), and immunohistochemistry as described previously (16, 44–46). We visualized perineuronal nets using biotinylated Wisteria Floribunda Lectin (Vector; 1:1,000). First, we incubated sections in blocking buffer consisting of 0.1 M PBS and 5% BSA for 1 h at room temperature. Subsequently, free-floating sections were incubated at least overnight with the primary antibodies in 0.1 M PBS containing 1% BSA and 0.5% Triton-X (PBS-X). We used primary antibodies against PV (Swant; 1:5,000), Forkhead box protein P2 (Sigma; 1:500), NeuN (Servicebio; 1:1,000), and Purkinje cell protein 4 (Sigma; 1:500) (for details, see SI Appendix, Table S3). Next, sections were visualized with fluorescent secondary antibodies diluted in PBS-X and then mounted on gelatinized slides. All histological processing was performed with the experimenter being blind to whether the sections were from a shrew from the summer or winter group.

In Situ Hybridization. In situ hybridization was performed as described previously (47, 48). Digoxigenin (DIG)-labeled riboprobes were used for hybridization on 40- to 60-µm free-floating cryosections. Hybridization was performed overnight at 60 to 65 °C. Sections were washed at 60 to 65 °C twice in 2xSSC/50% Formamide/0.1% N-lauroylsarcosine, twice in 2xSSC/0.1% N-lauroylsarcosine at 37 °C for 20 min, and twice in 0.2xSSC/0.1% N-lauroylsarcosine at 37 °C for 20 min. Sections were blocked in MABT (pH = 7.5)/10% goat serum/1% blocking reagent (Roche, cat# 11096176001), incubated overnight with sheep anti-DIG-AP (1:1,000; Roche cat# 11093274910). After washing, staining was performed using NBT/BCIP in NTMT until satisfactory intensity was reached. Staining reaction was stopped with 10 mM EDTA in PBS. Sections were washed, dehydrated, and mounted with Eukitt Quick-hardening mounting medium (Sigma Aldrich).

Shrew cDNA was synthesized from total brain RNA using iScript Reverse Transcription Supermix (Bio-Rad Laboratories). Genes of interest were amplified by PCR with the primer pairs indicated in SI Appendix, Table S4 (Phusion, New England Biolabs). Primers were generated using the draft S. etruscus genome assembly generated by X. Liu, G. Ka-Shu Wong, and colleagues (Beijing Genomics Institute, Shenzhen, China). PCR fragments were individually cloned in pEASY-Blunt Zero backbone (Transgen Biotech) and verified by sequencing and comparison with the draft S. etruscus genome, as well as the genome of the closely related common shrew (Sorex araneus) (49). Antisense DIG-labeled riboprobes were synthesized according to the protocol recommended by the manufacturer (Roche Cat# 11277073910).

Image Acquisition. Chromogenic stainings were imaged at a 10× or 20× magnification using an Olympus BX51 microscope (Olympus) or slide scanner Olympus BX61VS (Olympus). Fluorescent sections were imaged using an inverted confocal microscope (LSM 880, Zeiss). The fluorescent images were acquired in monochrome and color maps were applied to the images post acquisition. Post hoc linear brightness and contrast adjustment were applied uniformly to the image under analysis.

Cortical Thickness, Cell Counts, and Fluorescence Intensity. The thickness of entire somatosensory cortex and different layers were measured using ImageJ. We chose three sections through the somatosensory cortex at ~1,320 µm, 1,560 µm, and 1,780 µm from the lateral edge of the cortex for measurement. In each section we measured thickness in the center of somatosensory cortex (~1,300-µm posterior from the posterior edge of the olfactory bulb) and 100-µm anterior and posterior to this central point to sample thickness systematically and evenly. Cortical layers were defined based on cell density in the Nissl staining and with the help of layer-specific markers (Fig. 2 and SI Appendix, Fig. S4). Comparisons of layer-specific markers (Fig. 2C and SI Appendix, Fig. S4A) and fluorescence intensities (SI Appendix, Fig. S4B) were made either directly to adjacent Nissl sections or with NeuN or DAPI costaining (Fig. 2F and SI Appendix, Fig. S4B), which were then compared to Nissl stains to confirm laminar borders. For neuron counting, 100-µm-wide columns from the somatosensory cortex region were selected from 60-µm-thick sagittal sections in 10 shrew brains stained for NeuN, PV, and wisteria floribunda agglutinin (WFA). The sections and locations of the central points of the columns, was determined in a similar to that for determining layer widths. We then counted neurons manually using the Cell Counter Plugin in ImageJ. We focused on layer 4, which was defined based on cell density and high levels of WFA expression. To aid locating layer 4, normalized WFA intensity related to distance was measured using plot profile in ImageJ (SI Appendix, Fig. S4B). We subsequently quantified NeuN, PV, and WFA+PV neuron number in layer 4. All anatomical analysis was performed with the experimenter being blind to whether the shrew was from the summer or winter group and cortical and layer thickness measurements were performed by two independent experts with the cumulative results being used, with their independent results being consistent with each other and with the cumulative results.

Dye Loading. Multicell bolus loading of neocortical cells with the calcium indicator Oregon Green BAPTA-1 (OGB-1) AM (Invitrogen) was performed as described previously (50, 51). Astrocytes were labeled with sulforhodamine 101 (0.1 mM). Injections were performed under visual guidance using two-photon excitation. For loading, OGB-1-AM (1 mM) was slowly (duration 1 to 3 min) pressure-ejected into deep cortical layers of the somatosensory cortex at 0.2 to 0.3 bar with the micropipette tip 400 to 500 µm below the pia. The micropipette was front-loaded with a dye solution containing OGB-1 dissolved in 5 µL 20% Pluronic F-127 in DMSO, 0.5 µL Alexa 593 to visualize the pipette tip in tissue and 150 mM NaCl, 2.5 mM KCl, and 10 mM Hepes.

Surgical Procedures for Two-Photon Microscopy. Preparation was performed as described previously (52). Briefly, shrews were anesthetized with an intraperitoneal injection of 45 µL 4% urethane for an adult ~2.5 g shrew. Depth of anesthesia was assessed by monitoring the toe pinch withdrawal reflex and additional doses of 20 µL 2% urethane were given as necessary. Body temperature was allowed to drop to ~27 °C during surgery. The skull was exposed, cleaned, and dried, and a metal plate was attached with dental acrylic cement. A 2-mm-wide craniotomy was opened above somatosensory cortex. The exposed cortex was superfused with warm normal rat Ringer's (NRR) solution: 135 mM NaCl, 5.4 mM KCl, 5 mM Hepes, 1 mM MgCl$_2$, and 1.8 mM CaCl$_2$, pH 7.2 with NaOH. The craniotomy was filled with agarose (type III-A [Sigma]; 1% in NRR) and covered with an immobilized glass coverslip.

Two-Photon Microscopy. Imaging was carried out on an Olympus FV1000 microscope (Olympus). Fluorescence images of 64×128 pixels were acquired with a 25× (1.05 NA) water-immersion objective (Olympus, XLPL25XWMP) at 4- to 10-Hz frame rate. A femtosecond laser (Mai-Tai Spectra Physics) was used to excite OGB-1 at 870 nm. Imaging started 45-min postinjection and lasted for up to 3 h.

Whisker Stimulation. Whisker responses were assessed with piezoelectric stimulation of single whiskers at the contralateral side of the snout. The whisker was selected prior to the start of the experiment based on the one eliciting the highest response to stimulation in the imaging region, to putatively determine the principal whisker corresponding to that cortical region. During the experiment, changes in imaging position were only made along the z-axis. Timestamps of whisker stimulation and image acquisition were fed into Spike2 for post hoc analysis.

Determination of Imaging Layer. Following each experiment, z-stacks were acquired of the imaged volume. Subsequently, animals were killed by overdose with urethane and perfused with 4% PFA for histology. Images of the perfused brain surface were matched to the z-stacks using the blood vessel pattern to confirm location in somatosensory cortex. Furthermore, brains were processed for alternating Nissl and cytochrome oxidase staining and imaging locations were confirmed based on blood vessel pattern and position of faint reductions in cytochrome oxidase staining for precise laminar alignment (*SI Appendix*, Fig. S6) (53).

Extraction of Fluorescence Signals. Regions of interest were drawn only around well-focused cell bodies (judged from the diameter compared to 3D image stacks containing the imaged neurons) because out-of-focus neurons showed reduced signal-to-noise, lowering spike detection reliability. Baseline fluorescence (F0) was defined as the mean of the lowest 50% of fluorescence values measured within 10 s before or after each frame and used to calculate ΔF/F0 for each frame, as described previously (54, 55). Spike events were estimated from the calcium transients using a maximal likelihood approach by the MLSpike algorithm (56). Cells were z-scored on the basis of their responses to tactile stimuli provided at random intervals by a piezoelectric actuator, considering stimuli that were provided at least at 4-s intervals and having a minimum of five repetitions.

Data Inclusion Criteria. All data were included for MRI and anatomical experiments. For two-photon imaging experiments, one video was excluded due to motion artifacts during recording that could not be corrected on stabilization. Neurons that showed no activity during the entire period ($n = 132$) were also excluded.

Statistical Analysis. With repeated measurements of brain and substructure volume in MRI measurements, one-way repeated-measure ANOVA was performed. Furthermore, two-tailed paired t test was conducted for pairs passing normality check by Shapiro–Wilk test, with Bonferroni correction being applied for multiple comparisons where appropriate. To determine effect size, Cohen's d was calculated (57, 58). For differences between suppressed and activated neurons in summers and winters determined by two-photon imaging, a two-proportion z-test and χ^2 test was performed. For comparison of cortical layer widths and cell counts we performed two-tailed Mann–Whitney U test, with Bonferroni correction being applied for multiple comparisons where appropriate.

Data Availability. All data necessary to support the paper's conclusions are present in the main text and *SI Appendix*. The resulting average shrew brain template, based on 48 shrew brain scans, was processed with ANTX2 and is publicly available on GitHub (https://github.com/ChariteExpMri/antx2).

1. C. V. Riley, On migratory butterflies. *J. Proc. Acad. Sci. St. Louis* **3**, cclxxiii–cclxxiv (1878).
2. E. T. Pengelley, K. C. Fisher, Onset and cessation of hibernation under constant temperature and light in the golden-mantled ground squirrel (Citellus lateralis). *Nature* **180**, 1371–1372 (1957).
3. M. E. Diamond, M. Armstrong-James, F. F. Ebner, Experience-dependent plasticity in adult rat barrel cortex. *Proc. Natl. Acad. Sci. U.S.A.* **90**, 2082–2086 (1993).
4. J. H. Kaas et al., Reorganization of retinotopic cortical maps in adult mammals after lesions of the retina. *Science* **248**, 229–231 (1990).
5. D. E. Feldman, M. Brecht, Map plasticity in somatosensory cortex. *Science* **310**, 810–815 (2005).
6. R. G. M. Morris, E. Anderson, G. S. Lynch, M. Baudry, Selective impairment of learning and blockade of long-term potentiation by an N-methyl-D-aspartate receptor antagonist, AP5. *Nature* **319**, 774–776 (1986).
7. F. Nottebohm, A brain for all seasons: Cyclical anatomical changes in song control nuclei of the canary brain. *Science* **214**, 1368–1370 (1981).
8. M. A. Hofman, D. F. Swaab, Seasonal changes in the suprachiasmatic nucleus of man. *Neurosci. Lett.* **139**, 257–260 (1992).
9. S. D. Briscoe, C. W. Ragsdale, Homology, neocortex, and the evolution of developmental mechanisms. *Science* **362**, 190–193 (2018).
10. M. A. Tosches et al., Evolution of pallium, hippocampus, and cortical cell types revealed by single-cell transcriptomics in reptiles. *Science* **360**, 881–888 (2018).
11. A. Dehnel, Studies on the genus Sorex L. *Ann Univ Marie Curie Sklodowska Sect C.* **4**, 17–102 (1949).
12. D. K. Dechmann et al., Profound seasonal shrinking and regrowth of the ossified braincase in phylogenetically distant mammals with similar life histories. *Sci. Rep.* **7**, 42443 (2017).
13. M. Pucek, Water contents and seasonal changes of the brain-weight in shrews. *Acta Theriol. (Warsz.)* **10**, 353–367 (1965).
14. J. Lázaro, D. K. N. Dechmann, S. LaPoint, M. Wikelski, M. Hertel, Profound reversible seasonal changes of individual skull size in a mammal. *Curr. Biol.* **27**, R1106–R1107 (2017).
15. J. Lázaro, M. Hertel, M. Muturi, D. K. N. Dechmann, Seasonal reversible size changes in the braincase and mass of common shrews are flexibly modified by environmental conditions. *Sci. Rep.* **9**, 2489 (2019).
16. R. K. Naumann, F. Anjum, C. Roth-Alpermann, M. Brecht, Cytoarchitecture, areas, and neuron numbers of the Etruscan shrew cortex. *J. Comp. Neurol.* **520**, 2512–2530 (2012).
17. F. Anjum, H. Turni, P. G. Mulder, J. van der Burg, M. Brecht, Tactile guidance of prey capture in Etruscan shrews. *Proc. Natl. Acad. Sci. U.S.A.* **103**, 16544–16549 (2006).
18. M. Brecht et al., The neurobiology of Etruscan shrew active touch. *Philos. Trans. R. Soc. Lond. B Biol. Sci.* **366**, 3026–3036 (2011).
19. K. Fox, *Barrel Cortex* (Cambridge University Press, 2008).
20. T. A. Woolsey, C. Welker, R. H. Schwartz, Comparative anatomical studies of the SmI face cortex with special reference to the occurrence of "barrels" in layer IV. *J. Comp. Neurol.* **164**, 79–94 (1975).
21. K. C. Catania, D. C. Lyon, O. B. Mock, J. H. Kaas, Cortical organization in shrews: Evidence from five species. *J. Comp. Neurol.* **410**, 55–72 (1999).
22. E. K. Sawyer, E. C. Turner, J. H. Kaas, Somatosensory brainstem, thalamus, and cortex of the California sea lion (Zalophus californianus). *J. Comp. Neurol.* **524**, 1957–1975 (2016).
23. M. T. Wong-Riley, Cytochrome oxidase: An endogenous metabolic marker for neuronal activity. *Trends Neurosci.* **12**, 94–101 (1989).
24. C. Koelbl, M. Helmstaedter, J. Lübke, D. Feldmeyer, A barrel-related interneuron in layer 4 of rat somatosensory cortex with a high intrabarrel connectivity. *Cereb. Cortex* **25**, 713–725 (2015).
25. O. Kann, I. E. Papageorgiou, A. Draguhn, Highly energized inhibitory interneurons are a central element for information processing in cortical networks. *J. Cereb. Blood Flow Metab.* **34**, 1270–1282 (2014).
26. R. Tremblay, S. Lee, B. Rudy, GABAergic interneurons in the neocortex: From cellular properties to circuits. *Neuron* **91**, 260–292 (2016).
27. F. Donato, S. B. Rompani, P. Caroni, Parvalbumin-expressing basket-cell network plasticity induced by experience regulates adult learning. *Nature* **504**, 272–276 (2013).
28. M. Wikelski, C. Thom, Marine iguanas shrink to survive El Niño. *Nature* **403**, 37–38 (2000).
29. C. M. Donihue et al., Hurricane-induced selection on the morphology of an island lizard. *Nature* **560**, 88–91 (2018).
30. I. Saavedra, L. Amo, Insectivorous birds eavesdrop on the pheromones of their prey. *PLoS One* **13**, e0190415 (2018).
31. E. Gwinner, *Circannual Rhythms. Endogenous Annual Clocks in the Organization of Seasonal Processes* (Springer-Verlag, 1986).
32. N. Mattugini et al., Inducing different neuronal subtypes from astrocytes in the injured mouse cerebral cortex. *Neuron* **103**, 1086–1095.e5 (2019).
33. P. Vogel, "Metabolic levels and biological strategies in shrews" in *Comparative Physiology: Primitive Mammals*, K. Schmidt-Nielsen, L. Bolis, C. R. Taylor, Eds. (Cambridge University Press, 1980), pp. 170–180.

NEUROSCIENCE

34. W. J. Schwartz, F. R. Sharp, Autoradiographic maps of regional brain glucose consumption in resting, awake rats using (14C) 2-deoxyglucose. *J. Comp. Neurol.* **177**, 335–359 (1978).

35. R. N. Sachdev, M. R. Krause, J. A. Mazer, Surround suppression and sparse coding in visual and barrel cortices. *Front. Neural Circuits* **6**, 43 (2012).

36. S. Churchfield, L. Rychlik, J. R. Taylor, Food resources and foraging habits of the common shrew, Sorex araneus: Does winter food shortage explain Dehnel's phenomenon? *Oikos* **121**, 1593–1602 (2012).

37. P. H. Harvey, Optimal foraging: When the going gets tough. *Nature* **317**, 388–389 (1985).

38. S. Koch *et al*., Atlas registration for edema-corrected MRI lesion volume in mouse stroke models. *J. Cereb. Blood Flow Metab.* **39**, 313–323 (2019).

39. S. Klein, M. Staring, K. Murphy, M. A. Viergever, J. P. Pluim, elastix: A toolbox for intensity-based medical image registration. *IEEE Trans. Med. Imaging* **29**, 196–205 (2010).

40. K. Hikishima *et al*., In vivo microscopic voxel-based morphometry with a brain template to characterize strain-specific structures in the mouse brain. *Sci. Rep.* **7**, 85 (2017).

41. J. Ashburner, K. J. Friston, Unified segmentation. *Neuroimage* **26**, 839–851 (2005).

42. L. R. Dice, Measures of the amount of ecologic association between species. *Ecology* **26**, 297–302 (1945).

43. M. F. Glasser *et al*., A multi-modal parcellation of human cerebral cortex. *Nature* **536**, 171–178 (2016).

44. P. Beed *et al*., Species-specific differences in synaptic transmission and plasticity. *Sci. Rep.* **10**, 16557 (2020).

45. S. Ray *et al*., Grid-layout and theta-modulation of layer 2 pyramidal neurons in medial entorhinal cortex. *Science* **343**, 891–896 (2014).

46. S. Ray, A. Burgalossi, M. Brecht, R. K. Naumann, Complementary modular microcircuits of the rat medial entorhinal cortex. *Front. Syst. Neurosci.* **11**, 20 (2017).

47. K. Song *et al*., The TRPM2 channel is a hypothalamic heat sensor that limits fever and can drive hypothermia. *Science* **353**, 1393–1398 (2016).

48. A. M. Clemens *et al*., Estrus-cycle regulation of cortical inhibition. *Curr. Biol.* **29**, 605–615.e6 (2019).

49. K. Lindblad-Toh *et al*.; Broad Institute Sequencing Platform and Whole Genome Assembly Team; Baylor College of Medicine Human Genome Sequencing Center Sequencing Team; Genome Institute at Washington University, A high-resolution map of human evolutionary constraint using 29 mammals. *Nature* **478**, 476–482 (2011).

50. C. Stosiek, O. Garaschuk, K. Holthoff, A. Konnerth, In vivo two-photon calcium imaging of neuronal networks. *Proc. Natl. Acad. Sci. U.S.A.* **100**, 7319–7324 (2003).

51. J. N. Kerr, D. Greenberg, F. Helmchen, Imaging input and output of neocortical networks in vivo. *Proc. Natl. Acad. Sci. U.S.A.* **102**, 14063–14068 (2005).

52. C. Roth-Alpermann, F. Anjum, R. Naumann, M. Brecht, Cortical organization in the Etruscan shrew (Suncus etruscus). *J. Neurophysiol.* **104**, 2389–2406 (2010).

53. A. K. Garg, P. Li, M. S. Rashid, E. M. Callaway, Color and orientation are jointly coded and spatially organized in primate primary visual cortex. *Science* **364**, 1275–1279 (2019).

54. D. S. Greenberg, A. R. Houweling, J. N. Kerr, Population imaging of ongoing neuronal activity in the visual cortex of awake rats. *Nat. Neurosci.* **11**, 749–751 (2008).

55. D. S. Greenberg, J. N. Kerr, Automated correction of fast motion artifacts for two-photon imaging of awake animals. *J. Neurosci. Methods* **176**, 1–15 (2009).

56. T. Deneux *et al*., Accurate spike estimation from noisy calcium signals for ultrafast three-dimensional imaging of large neuronal populations in vivo. *Nat. Commun.* **7**, 12190 (2016).

57. J. Cohen, *Statistical Power Analysis for the Behavioral Sciences* (Routledge, New York, 1988).

58. S. Sawilowsky, New effect size rules of thumb. *J. Mod. Appl. Stat. Methods* **8**, 467–474 (2009).